Hysteretic Superconducting Heat-Flux Quantum Modulator

Claudio Guarcello,[1,2,3,*] Paolo Solinas,[1,†] Massimiliano Di Ventra,[4,‡] and Francesco Giazotto[2,§]

[1]*SPIN-CNR, Via Dodecaneso 33, 16146 Genova, Italy*
[2]*NEST, Istituto Nanoscienze-CNR and Scuola Normale Superiore,*
Piazza San Silvestro 12, I-56127 Pisa, Italy
[3]*Radiophysics Department, Lobachevsky State University,*
Gagarin Avenue 23, 603950 Nizhni Novgorod, Russia
[4]*Department of Physics, University of California, San Diego, La Jolla, California 92093, USA*

We discuss heat transport in a thermally biased superconducting quantum-interference device (SQUID) in the presence of an external magnetic flux, when a non-negligible inductance of the SQUID ring is taken into account. A properly sweeping driving flux causes the thermal current to modulate and behave hysteretically. The response of this device is analyzed as a function of both the hysteresis parameter and the degree of asymmetry of the SQUID, highlighting the parameter range over which hysteretic behavior is observable. Markedly, the temperature of the SQUID also shows hysteretic evolution, with sharp transitions characterized by temperature jumps up to, e.g., approximately 0.02 K for a realistic Al-based setup. In view of these results, the proposed device can effectively find an application as a temperature-based superconducting memory element, working even at gigahertz frequencies by suitably choosing the superconductor on which the device is based.

I. INTRODUCTION

In 1965, Maki and Griffin [1] predicted that, in a temperature-biased Josephson junction (JJ), the flow of an electronic heat current should depend on the macroscopic phase difference between the superconductors forming the junction. Recently, the features of the phase-coherent thermal transport in Josephson devices have been investigated and confirmed experimentally in several interferometerlike structures [2–9]. In Ref. [2], for instance, the thermal counterpart of a symmetric dc superconducting quantum-interference device (SQUID) with negligible inductance of the loop was demonstrated. The heat current flowing through a thermally biased SQUID depends on the external magnetic flux Φ, i.e., $\propto |\cos(\pi\Phi/\Phi_0)|$. In Ref. [2], clear modulations of the drain temperature as a function of Φ were observed, due to the interference between the coherent components of the heat currents flowing throughout the JJs forming the SQUID. The coherent nature of the thermal current was further confirmed in Ref. [5] by the observation of thermal diffraction patterns in a flux-driven, temperature-biased "short" rectangular tunnel JJ. When a temperature-biased extended JJ is threaded by a magnetic flux, a Fraunhofer-like diffraction pattern, i.e., $\propto |\sin(\pi\Phi/\Phi_0)/(\pi\Phi/\Phi_0)|$, for the drain temperature is observed [5].

In this paper, we theoretically investigate the thermal transport in a temperature-biased SQUID with a non-negligible ring inductance, as a slowly changing external magnetic flux (i.e., in the adiabatic regime) is taken into account. We show that hysteresis in the thermal current comes to light for proper values of the system parameters. By considering a simple thermal model accounting for the thermal currents flowing into and from the cold electrode of the SQUID [10], the modulation due to the external flux of its temperature in both nonhysteretic—i.e., with vanishing inductance—and hysteretic regimes is explored. Notably, we predict that the temperature also behaves hysteretically, showing sudden transitions as the number of enclosed flux quanta in the SQUID ring changes. When this behavior occurs, clear thermal jumps of up to $\Delta T_2 \sim 0.02$ K are observed.

The paper is organized as follows. In Sec. II, the theoretical background used to describe a thermally biased SQUID is presented. The thermal currents are introduced and studied by varying the values of appropriate parameters, for several temperatures of the SQUID branches. In Sec. III, the behavior of the temperature of the cold electrode of the SQUID is explored, as the thermal contact with bath phonons is taken into account. In Sec. IV, conclusions are drawn.

II. MODEL AND RESULTS

The device we are discussing is a double-tunnel-junction superconducting quantum-interference device, namely, a dc SQUID, formed by two superconductors S_1 and S_2 in a thermal steady state residing at different temperatures T_1

*claudio.guarcello@nano.cnr.it
†paolo.solinas@spin.cnr.it
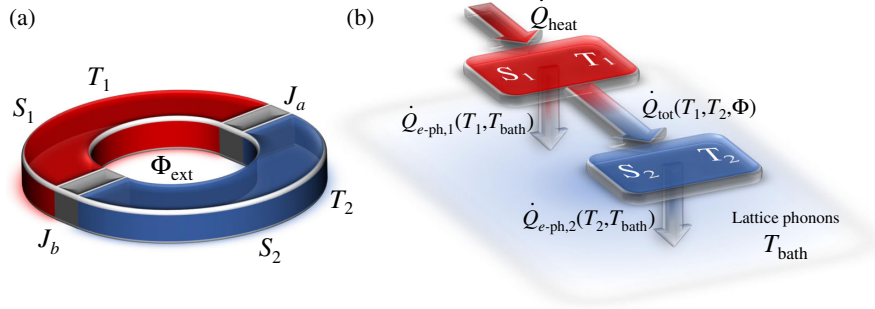‡diventra@physics.ucsd.edu
§giazotto@sns.it

FIG. 1.   (a) Two superconductors S_1 and S_2, kept at temperatures T_1 and T_2 (with $T_1 \geq T_2$), respectively, are tunnel coupled through the junctions J_a and J_b so as to implement a dc SQUID. Φ_{ext} is the applied magnetic flux threading the SQUID loop. (b) Sketch of the thermal model accounting for heat transport in the system. The total heat current, $\dot{Q}_{\text{tot}}$, flowing in the system depends on the temperatures and the total flux Φ [see Eq. (12)] through the SQUID ring. $\dot{Q}_{e\text{-ph},i}(T_i, T_{\text{bath}})$ represents the coupling between quasiparticles in S_i and the lattice phonons residing at T_{bath}, whereas $\dot{Q}_{\text{heat}}$ denotes the power injected into S_1 through heating probes in order to impose a quasiparticle temperature T_1. The arrows indicate the direction of heat currents for $T_{\text{bath}} < T_2 < T_1$.

and T_2, respectively, with $T_1 \geq T_2$ [see Fig. 1(a)]. In the presence of a temperature gradient and with no voltage bias, a stationary finite heat current, $\dot{Q}_{\text{tot}}$, given by

$$\dot{Q}_{\text{tot}}(T_1, T_2) = \dot{Q}_{\text{qp}}(T_1, T_2) - \dot{Q}_{\text{int}}(T_1, T_2, \varphi_a, \varphi_b), \quad (1)$$

flows from S_1 to S_2 [1,10–15], see Fig. 1. Equation (1) contains the interplay between Cooper pairs and quasiparticles in tunneling through a JJ predicted by Maki and Griffin [1]. In fact, the term

$$\dot{Q}_{\text{qp}} = \dot{Q}_{\text{qp}}^a(T_1, T_2) + \dot{Q}_{\text{qp}}^b(T_1, T_2) \quad (2)$$

is the heat flux carried by quasiparticles and represents an incoherent flow of energy from the hot to the cold electrode [1,16,17] through the junctions J_a and J_b. Instead, the term

$$\dot{Q}_{\text{int}} = \dot{Q}_{\text{int}}^a(T_1, T_2) \cos \varphi_a + \dot{Q}_{\text{int}}^b(T_1, T_2) \cos \varphi_b \quad (3)$$

is the phase-dependent part of the heat current [1,11,13–15] (with $\varphi_{a(b)}$ being the macroscopic quantum phase difference between the superconductors across the junction $J_{a(b)}$). It is peculiar to the tunnel JJs forming the SQUID and is the thermal counterpart of the "quasiparticle-pair interference" term contributing to the electrical current tunneling through a JJ [18]. This term originates from the energy-carrying tunneling processes involving recombination and destruction of Cooper pairs on both sides of each junction, and it is therefore governed by the phase difference $\varphi_{a(b)}$ between the two superconducting condensates. The oscillatory behavior of the thermal current was experimentally verified in Refs. [2,5,7].

The terms of Eq. (2) explicitly read [1,11–15]

$$\dot{Q}_{\text{qp}}^{a(b)} = \frac{1}{e^2 R_{a(b)}} \int_0^\infty d\varepsilon \varepsilon \mathcal{N}_1(\varepsilon, T_1) \mathcal{N}_2(\varepsilon, T_2)$$
$$\times [f(\varepsilon, T_2) - f(\varepsilon, T_1)], \quad (4)$$

where

$$\mathcal{N}_i(\varepsilon, T_i) = \left| \text{Re} \left(\frac{\varepsilon + i\Gamma_i}{\sqrt{(\varepsilon + i\Gamma_i)^2 - \Delta_i(T_i)^2}} \right) \right| \quad (5)$$

is the smeared normalized BCS density of states in S_i at temperature T_i ($i = 1, 2$), which Γ_i being the Dynes parameter [19]. Hereafter, we set $\Gamma_i = 10^{-4} \Delta_i(0)$, a value which describes realistic superconducting tunnel junctions [20,21]. Here, ε is the energy measured from the condensate chemical potential, $\Delta_i(T_i)$ is the temperature-dependent superconducting energy gap, $f(\varepsilon, T_i) = \tanh(\varepsilon / 2k_B T_i)$, $R_{a(b)}$ is the junction normal-state resistance, k_B is the Boltzmann constant, and e is the electron charge. The terms of Eq. (3) read [1,11–15]

$$\dot{Q}_{\text{int}}^{a(b)} = \frac{1}{e^2 R_{a(b)}} \int_0^\infty d\varepsilon \varepsilon \mathcal{M}_1(\varepsilon, T_1) \mathcal{M}_2(\varepsilon, T_2)$$
$$\times [f(\varepsilon, T_2) - f(\varepsilon, T_1)], \quad (6)$$

where

$$\mathcal{M}_i(\varepsilon, T_i) = \left| \text{Im} \left(\frac{-i\Delta_i(T_i)}{\sqrt{(\varepsilon + i\Gamma_i)^2 - \Delta_i(T_i)^2}} \right) \right| \quad (7)$$

is the Cooper pair BCS density of states in S_i at temperature T_i [18]. We note that both $\dot{Q}_{\text{qp}}^{a(b)}$ and $\dot{Q}_{\text{int}}^{a(b)}$ vanish for

$T_1 = T_2$, while $\dot{Q}_{\text{int}}^{a(b)}$ also vanishes when at least one of the superconductors is in the normal state, i.e., $\Delta_i(T_i) = 0$.

According to the conservation of the supercurrent circulating in the loop, the phases φ_a and φ_b satisfy the equation

$$I = I_J^a \sin \varphi_a = I_J^b \sin \varphi_b. \tag{8}$$

Here, $I_J^{a(b)}(T_1, T_2)$ is the critical current for the temperature-biased junction $J_{a(b)}$, given by [22–24]

$$I_J^{a(b)}(T_1, T_2) = \frac{1}{2eR_{a(b)}} \left| \int_{-\infty}^{\infty} \{ f(\varepsilon, T_1) \text{Re}[\mathfrak{F}_1(\varepsilon)] \text{Im}[\mathfrak{F}_2(\varepsilon)] \right.$$

$$\left. + f(\varepsilon, T_2) \text{Re}[\mathfrak{F}_2(\varepsilon)] \text{Im}[\mathfrak{F}_1(\varepsilon)] \} d\varepsilon \right|, \tag{9}$$

where $\mathfrak{F}_j(\varepsilon) = \Delta_j(T_j) / \sqrt{(\varepsilon + i\Gamma_j)^2 - \Delta_j^2(T_j)}$. In the following, we assume $\Delta_1(0) = \Delta_2(0) = \Delta = 1.764 k_B T_c$, with T_c being the common critical temperature of the superconductors. An in-plane external magnetic field also causes the JJ's critical current to modulate [18]. However, since the area of the SQUID ring is usually greater than the area of the junctions, this modulation occurs on a field scale much larger than the modulation period of thermal currents in the SQUID. Moreover, JJs in the so-called overlap geometry are usually preferred in SQUID-based applications [5], so that the magnetic field threading the loop is out of plane to the junction's area and no modulation of the critical currents occurs. Therefore, the junction critical currents I_J are assumed hereafter to be independent of the external flux variations.

The degree of asymmetry of the SQUID, α, is defined as the critical current's ratio, so that

$$\alpha = \frac{I_J^a}{I_J^b} = \frac{R_b}{R_a} = \frac{\dot{Q}_{\text{qp}}^a}{\dot{Q}_{\text{qp}}^b} = \frac{\dot{Q}_{\text{int}}^a}{\dot{Q}_{\text{int}}^b}, \tag{10}$$

according to Eqs. (4), (6), and (9). The flux quantization imposes the constraint

$$\varphi_a + \varphi_b + 2\pi \frac{\Phi}{\Phi_0} = 2\pi k, \tag{11}$$

where $\Phi_0 \simeq 2.067 \times 10^{-15}$ Wb is the flux quantum and k is an integer representing the amount of enclosed flux quanta, so that the transition $k \to k \pm 1$ indicates a variation of one flux quantum through the SQUID ring. In Eq. (11), Φ is the total magnetic flux given by

$$\Phi = \Phi_{\text{ext}} + LI, \tag{12}$$

where Φ_{ext} is the externally applied magnetic flux through the ring [see Fig. 1(a)] and the SQUID inductance L has a

geometric contribution as well as a kinetic contribution [25,26]. From Eqs. (8), (10), and (11), one obtains the circulating current, in units of I_J^a, as a function of the total flux [27]

$$\frac{I}{I_J^a} = \sin \varphi_a = \frac{-\sin(2\pi \frac{\Phi}{\Phi_0})}{\sqrt{1 + \alpha^2 + 2\alpha \cos(2\pi \frac{\Phi}{\Phi_0})}}, \tag{13}$$

so that, from Eq. (12), we obtain

$$\frac{\Phi}{\Phi_0} = \frac{\Phi_{\text{ext}}}{\Phi_0} - \frac{\beta \sin(2\pi \frac{\Phi}{\Phi_0})}{2\pi \sqrt{1 + \alpha^2 + 2\alpha \cos(2\pi \frac{\Phi}{\Phi_0})}}, \tag{14}$$

with $\beta = 2\pi L I_J^a / \Phi_0$ being the hysteresis parameter.

Before exploring the behavior of the total heat current by changing the temperatures of the electrodes T_1 and T_2, we observe that the hysteretic parameter β depends on them through the critical current I_J^a, according to Eq. (9). As is clearly shown in Fig. 2, $\beta(T_1, T_2) \to 0$ as the temperatures approach T_c, so the hysteresis reduces by increasing the temperature. In the following, a temperature-dependent hysteretic parameter is taken into account and the notation $\beta \equiv \beta(0, 0)$ is used.

When $\alpha \to 0$ (i.e., a single-junction SQUID) and $\alpha \to 1$ (i.e., a symmetric SQUID), Eq. (14) turns into $\Phi = \Phi_{\text{ext}} - LI_J^a \sin(2\pi \Phi / \Phi_0)$ and $\Phi = \Phi_{\text{ext}} - LI_J^a \sin(\pi \Phi / \Phi_0)$, respectively.

For proper values of α and β, the total flux Φ is a multivalued function of Φ_{ext} and the SQUID behaves hysteretically [27]. Specifically, for $\beta < 1 - \alpha$, the slope of Φ is always positive and the Φ vs Φ_{ext} plot is non-hysteretic [see the dashed curves in Fig. 3(a)]. Conversely, for $\beta > 1 - \alpha$, the slope of Φ switches from positive to negative, so that Φ vs Φ_{ext} is multivalued and a hysteretic curve results [see Fig. 3(a)]. Moreover, by increasing the values of β and α, the range of Φ_{ext} values in which Φ has negative slopes enlarges, and, accordingly, the hysteresis of the Φ vs Φ_{ext} curves is more pronounced; see Figs. 3(a) and 3(b), respectively.
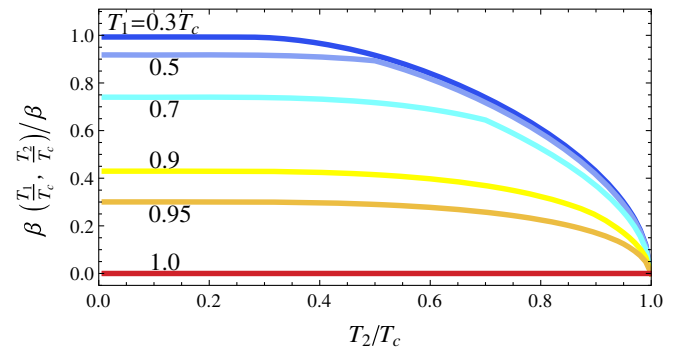

FIG. 2. Hysteresis parameter $\beta(T_1/T_c, T_2/T_c)$, in units of $\beta \equiv \beta(0, 0)$, as a function of the normalized temperature T_2/T_c, for a few values of T_1/T_c.
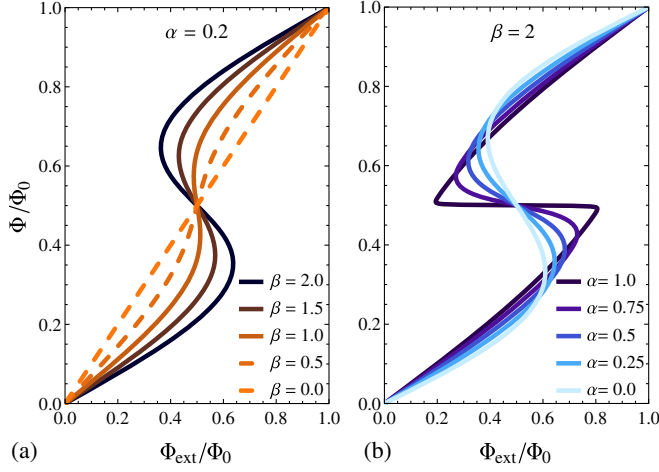
FIG. 3. Normalized total magnetic flux Φ/Φ_0 as a function of the normalized external magnetic flux Φ_{ext}/Φ_0 for $\alpha = 0.2$ and several values of β [see (a)], and for $\beta = 2$ and several values of α [see (b)]. Dashed curves represent nonhysteretic conditions.

The adiabatic evolution of the system is obtained from the minimization of the free energy of the SQUID, which is composed of the Josephson energies and the inductive energy, due to the screening current flowing into the SQUID ring,

$$E = -\frac{\Phi_0}{2\pi}(I_J^a \cos\varphi_a + I_J^b \cos\varphi_b) + \frac{1}{2}LI^2. \quad (15)$$

From Eqs. (8) and (13), the free energy (in units of $E_J = (\Phi_0/2\pi)I_J^a$) becomes

$$\frac{E}{E_J} = -\frac{1}{\alpha}\sqrt{1 + \alpha^2 + 2\alpha\cos\left(2\pi\frac{\Phi}{\Phi_0}\right)}$$

$$+ \frac{\beta}{2}\frac{\sin^2\left(2\pi\frac{\Phi}{\Phi_0}\right)}{1 + \alpha^2 + 2\alpha\cos\left(2\pi\frac{\Phi}{\Phi_0}\right)}. \quad (16)$$

The hysteretic behaviors of the total flux, the normalized Josephson current, and the free energy of a SQUID with $\alpha = 0.25$ and $\beta = 2$ are shown in Figs. 4(a), 4(b), and 4(c), respectively. The effect of the inductance is evident in Fig. 4(a), where the total flux Φ grows less rapidly than Φ_{ext} for the flux generated by the screening current that opposes Φ_{ext}. As $|I|$ exceeds the critical value I_J^a [see Fig. 4(b)], the junction temporarily switches into the voltage state [18]. Correspondingly, a jump to a lower free energy occurs [see Fig. 4(c)] and the SQUID undergoes a quantum transition $k \to k+1$, so that the flux through the SQUID changes by one flux quantum [see Fig. 4(a)]. Further reducing the external flux, the system remains in the $k = 1$ state until the circulating current $|I|$ reaches the critical value I_J^a and the free energy jumps again to a lower value, when the SQUID switches to the $k = 0$
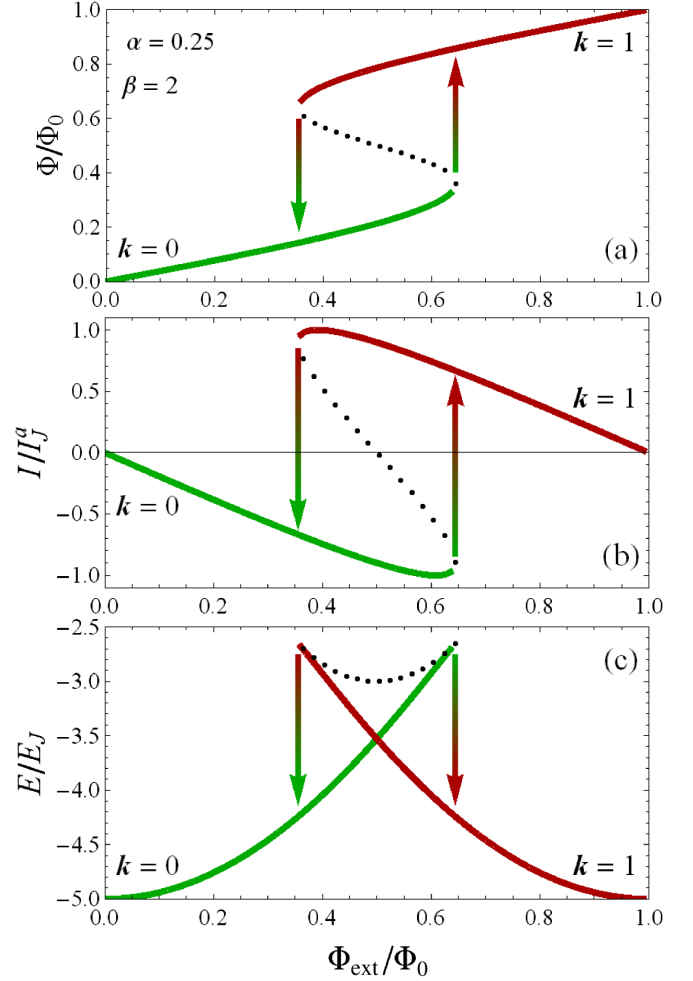

FIG. 4. Normalized total flux, normalized supercurrent, and free energy of the SQUID as a function of the external flux Φ_{ext}/Φ_0 [see (a), (b), and (c), respectively] for $\alpha = 0.25$ and $\beta = 2$. Arrows indicate the transition between quantum states with different numbers k of flux quanta penetrating the loop. Dotted curves represent the unstable states in the hysteretic mode.

state. We note that, for negative slopes of Φ (the dotted curves in Fig. 4), the SQUID free energy is definitively higher with respect to the energies of the states for positive Φ slopes. Therefore, the states corresponding to negative Φ slopes (the dotted curves in Fig. 4) are definitively unstable and are not observed during an adiabatic evolution, so that, in sweeping Φ_{ext} back and forth, a hysteretic path is traced out. Hereafter, dotted curves in the figures represent unstable states of the SQUID.

According to Eqs. (8) and (13), one gets [27]

$$\cos\varphi_a = \frac{\alpha + \cos\left(2\pi\frac{\Phi}{\Phi_0}\right)}{\sqrt{1 + \alpha^2 + 2\alpha\cos\left(2\pi\frac{\Phi}{\Phi_0}\right)}} \quad (17)$$

$$\cos\varphi_b = \frac{1 + \alpha\cos\left(2\pi\frac{\Phi}{\Phi_0}\right)}{\sqrt{1 + \alpha^2 + 2\alpha\cos\left(2\pi\frac{\Phi}{\Phi_0}\right)}}, \quad (18)$$
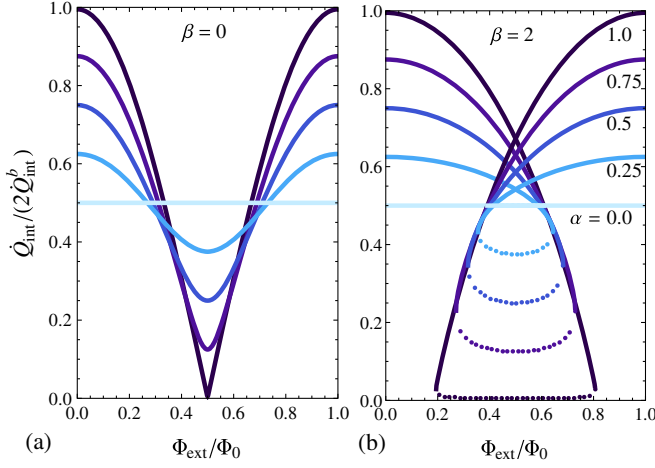
FIG. 5. Interference heat current $\dot{Q}_{\text{int}}$ as a function of the normalized external magnetic flux Φ_{ext}/Φ_0, for several values of α, for $\beta = 0.0$ and $\beta = 2$; see (a) and (b), respectively. Here, we set generic temperatures T_1 and T_2, such that $T_2 < T_1 < T_c$. Dotted curves represent the unstable states in the hysteretic mode.

FIG. 6. Total heat current $\dot{Q}_{\text{tot}}$ as a function of the normalized external magnetic flux Φ_{ext}/Φ_0 for a few values of T_1 and $T_2 = 0.1T_c$, assuming that $\alpha = 0.75$, for $\beta = 0.0$ and $\beta = 2$; see (a) and (b), respectively. Dotted curves represent the unstable states in the hysteretic mode.

so that $\dot{Q}_{\text{int}}$ [see Eq. (3)] becomes [10]

$$\dot{Q}_{\text{int}} = \dot{Q}_{\text{int}}^b(T_1, T_2)\sqrt{1 + \alpha^2 + 2\alpha \cos\left(2\pi\frac{\Phi}{\Phi_0}\right)}. \quad (19)$$

The behavior of the interference heat current $\dot{Q}_{\text{int}}$, as a function of the external flux, for a few values of α and for $\beta = 0.0$ and $\beta = 2$ is shown in Figs. 5(a) and 5(b), respectively. Generic temperatures T_1 and T_2, such that $T_2 < T_1 < T_c$, are set. $\dot{Q}_{\text{int}}$ is a periodic function of the external flux, and it is modulated between the maximum, given by $\dot{Q}_{\text{int}}^M = \dot{Q}_{\text{int}}^b(1 + \alpha)$ for $\Phi_{\text{ext}} = n\Phi_0$, and the minimum value, given by $\dot{Q}_{\text{int}}^m = \dot{Q}_{\text{int}}^b(1 - \alpha)$ for $\Phi_{\text{ext}} = (n + 1/2)\Phi_0$ (where n is an integer). Therefore, the modulation amplitude of $\dot{Q}_{\text{int}}$ is totally suppressed for $\alpha = 0$, so high junction symmetry is required to maximize the heat-current modulation in the device. By increasing the hysteresis parameter β, $\dot{Q}_{\text{int}}$ is multivalued in a neighborhood of $\Phi_0/2$, so the dip in $\Phi_{\text{ext}} = \Phi_0/2$ for $\beta = 0.0$ is replaced by a loop whose width increases with increases in both β and α. We observe that the bottom of these loops [see the dotted curves in Fig. 5(b)] corresponds to the unstable states of the SQUID. We also note that the height of the hysteretic jumps increases for $\alpha \to 1$.

Figure 6 shows the total heat current $\dot{Q}_{\text{tot}}$ as a function of Φ_{ext} at $T_2 = 0.1T_c$ for several values of T_1, for $\beta = 0.0$ and $\beta = 2$, see Figs. 6(a) and 6(b), respectively. As expected, $\dot{Q}_{\text{tot}}(\Phi_{\text{ext}})$ is modulated with the same Φ_0 periodicity as $\dot{Q}_{\text{int}}$, but unlike the latter, it is minimized (maximized) for integer (half-integer) values of Φ_0, according to a minus sign in front of the φ-dependent term in Eq. (1). Similar to $\dot{Q}_{\text{int}}$, the hysteretic loop for $\beta > 0$ appears also in $\dot{Q}_{\text{tot}}$,
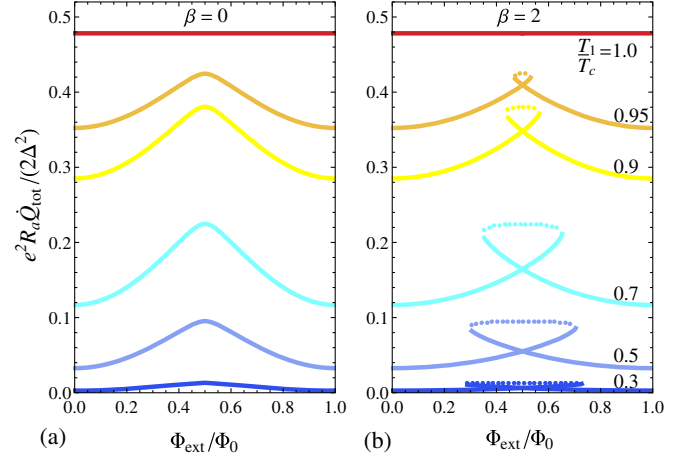
although the temperature dependence of the hysteresis parameter β makes the curves less and less hysteretic as $T_1 \to T_c$ [see Fig. 6(b)]. We observe that, at the lowest T_1, the total heat current is small, for $\dot{Q}_{\text{int}}$ and $\dot{Q}_{\text{qp}}$ are almost comparable. The total heat-current modulation amplitude, $\delta\dot{Q}_{\text{tot}}$, defined as the difference between the maximum and minimum values of $\dot{Q}_{\text{tot}}$, reduces further by increasing T_1, and it vanishes for $T_1 = T_c$ when S_1 is driven into the normal state. In Fig. 7(a), the behavior of $\delta\dot{Q}_{\text{tot}}$ is shown for the values of α, β, and T_2 used to obtain the data in Fig. 6(b). Specifically, $\delta\dot{Q}_{\text{tot}}$ is a nonmonotonic function vanishing for $T_1 = T_c$, with a maximum corresponding to an intermediate temperature depending on T_2. Specifically, by increasing T_2, the maximum value of $\delta\dot{Q}_{\text{tot}}$ reduces and shifts towards a higher T_1. Figure 7(b) shows the modulation amplitude $\delta\dot{Q}_{\text{tot}}$ at $T_2 = 0.1T_c$ for a few values of the asymmetry parameter α. Here, it is clearly shown that the modulation reduces with α, whereas the position of the maximum is not affected by α variations.

III. THERMAL MODEL

A practical experimental setup to observe thermal modulation was proposed in Ref. [10] and successfully implemented in Ref. [2]. The device consists of a tunnel-junction dc SQUID formed by identical superconductors, driven by a magnetic flux. Superconducting leads tunnel coupled to both SQUID electrodes, and serving either as heaters or thermometers (not shown in Fig. 1), allow us to perturb and to accurately probe the quasiparticle temperature in the structure [16]. The superconducting JJs provide nearly ideal thermal isolation of the SQUID electrodes [16] and, therefore, the thermal conductance through these probes can be neglected. The thermal model being
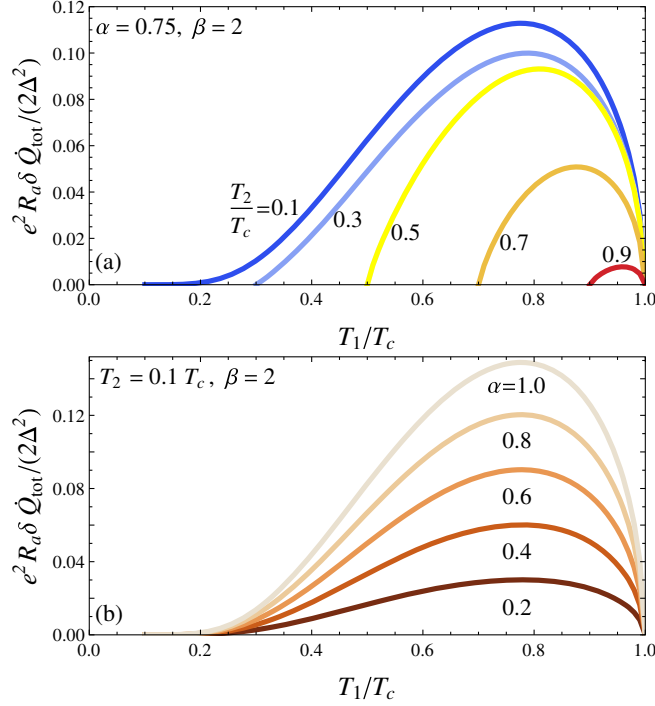
FIG. 7. Total heat-current modulation amplitude $\delta\dot{Q}_{tot}$ as a function of the normalized temperature T_1/T_c, assuming that $\beta = 2$, (a) for a few values of T_2 and when $\alpha = 0.75$, and (b) for a few values of α and $T_2 = 0.1T_c$.

discussed is sketched in Fig. 1(b). The steady temperature $T_2(\Phi)$ depends on the energy-relaxation mechanisms occurring in the electrode S_2. For any T_1, the thermal balance equation for the incoming and outgoing thermal currents in S_2 can be written as [10]

$$\dot{Q}_{tot}(T_1, T_2, \Phi) - \dot{Q}_{e\text{-ph},2}(T_2, T_{bath}) = 0. \qquad (20)$$

Here, the heat current flowing from S_1 is balanced by the electron-phonon interaction [16], $\dot{Q}_{e\text{-ph},2}$, namely, the predominant energy-relaxation mechanism in metals which allows energy exchange between the quasiparticles and the phonon bath. Specifically, $\dot{Q}_{e\text{-ph},i}$ in S_i reads [28]

$$\dot{Q}_{e\text{-ph},i} = \frac{-\Sigma \mathcal{V}_i}{96\zeta(5)k_b^5} \int_{-\infty}^{\infty} dE\, E \int_{-\infty}^{\infty} d\varepsilon\, \varepsilon^2 \text{sign}(\varepsilon) M_{E,E+\varepsilon}$$

$$\times \left\{ \coth\left(\frac{\varepsilon}{2k_b T_{bath}}\right) [f(E, T_i) - f(E + \varepsilon, T_i)] \right.$$

$$\left. - f(E, T_i) f(E + \varepsilon, T_i) + 1 \right\}, \qquad (21)$$

where $M_{E,E'} = \mathcal{N}_i(E, T_i)\mathcal{N}_i(E', T_i)[1 - \Delta^2(T_i)/(EE')]$, Σ is the electron-phonon coupling constant, $\mathcal{V}_i$ is the volume of S_i, and ζ is the Riemann ζ function. In the following calculations, an aluminium dc SQUID with bulk critical

temperature $T_c = 1.19$ K, $R_a = 1$ kΩ, $\mathcal{V}_2 = 10^{-19}$ m^3, and $\Sigma = 3 \times 10^8$ Wm^{-3} K^{-5} is taken into account.

The temperature T_2 of the electrode S_2 is obtained by solving Eq. (20). The behavior of T_2 by varying the flux Φ_{ext} for several temperatures T_1 at a fixed bath temperature $T_{bath} = 0.1$ K is shown in Figs. 8(a) and 8(b) for $\beta = 0.0$ and $\beta = 2$, respectively. The magnetic flux Φ_{ext} enclosed inside the SQUID ring modulates T_2 periodically, with a period of one flux quantum. By increasing T_1, the mean value of T_2 over a period increases. Markedly, the T_2 modulation amplitude, δT_2, defined as the difference between the maximum and the minimum value of T_2, behaves nonmonotonically by varying T_1. In fact, δT_2 is vanishing for low T_1's (specifically, for $T_1 = T_{bath}$, there is no thermal gradient along the system). It then increases up to $\delta T_2 \sim 35$ mK for $T_1 = 0.84$ K [see Fig. 8(a)], and it finally reduces again for $T_1 \to T_c$ due to the temperature-induced suppression of the energy gaps in the super-conductors. The flux modulation of T_2 in the hysteretic mode for $\beta = 2$ is shown in Fig. 8(b). The hysteretic behavior of the temperature T_2 as the flux Φ_{ext} is changed reflects the behavior of the total thermal current $\dot{Q}_{tot}$,
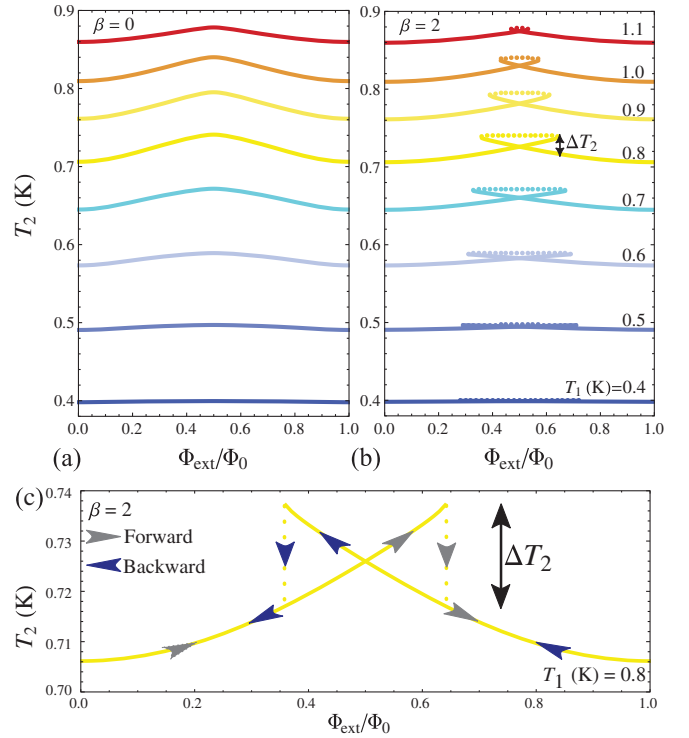

FIG. 8. Quasiparticle temperature T_2 vs Φ_{ext} calculated for a few values of T_1 at $T_{bath} = 0.1$ K for $\alpha = 0.75$, where $\beta = 0.0$ and $\beta = 2$ [(a) and (b), respectively]. Dotted curves represent the unstable states in the hysteretic mode. (c) The curve for $T_1 = 0.8$ K and $\beta = 2$, where arrows are used to trace forward and backward paths and indicate the transitions $k \to k \pm 1$ for a slow, varying external flux. (b),(c) indicate the height of a T_2 jump, ΔT_2, as Φ_{ext} induces a transition in the number of flux quanta through the SQUID ring, $k \to k \pm 1$.

although the temperature dependence of β clearly makes the curves less hysteretic as T_1 approaches T_c. The height of T_2 jumps, ΔT_2, as Φ_{ext} induces a transition in the number of flux quanta through the SQUID ring, $k \to k \pm 1$, enhances by increasing α and β. Instead, for a fixed α and β, it behaves nonmonotonically by varying T_1, just like δT_2 in the nonhysteretic mode. In fact, ΔT_2 vanishes for a low T_1 and for $T_1 \to T_c$, whereas it has a maximum $\Delta T_2 \sim 20$ mK for $T_1 = 0.84$ K [see Fig. 8(c)].

The role of the bath temperature is shown in Fig. 9, where $T_2(\Phi_{ext})$ is calculated for increasing T_{bath} at $T_1 = 1$ K, for $\beta = 0.0$ and $\beta = 2$, see Figs. 9(a) and 9(b), respectively. By increasing T_{bath}, the modulation of T_2 reduces, and it vanishes for $T_{bath} = T_1$; see Fig. 9(a). Accordingly, δT_2 decreases for $T_{bath} \to T_1$ since $\dot{Q}_{e\text{-ph},2}$ enhances, the temperature drop reduces, and the temperature-dependent energy gap in S_2 is suppressed. The hysteresis in $T_2(\Phi_{ext})$ is displayed in Fig. 9(b) for $\beta = 2$.

We observe that, at the temperatures we are considering, proper values for the system parameters have to be chosen to avoid the degradation of the SQUID sensitivity due to thermal fluctuations [26]. In fact, since the Josephson coupling energy E_J should be much larger than the thermal energy $k_B T$, a lower limit for the critical current exists, namely, $I_J/5 \gtrsim 2\pi k_b T/\Phi_0$ [26,29]. Moreover, Nyquist noise imposes an upper limit on the SQUID inductance, such that $5L \lesssim \Phi_0^2/(4\pi^2 k_b T)$ [26,29]. These constraints imply, for instance, $I_J \gtrsim 0.2$ μA and $L \lesssim 1.5$ nH at $T = 1$ K. Obviously, the value of the inductance depends on the applications in which the SQUID is employed. In fact, although a large area of the ring, corresponding to a large value of L, may deteriorate the SQUID performance, it is advantageous to increase the sensitivity of a SQUID-based magnetic-flux detector since small field variations give large flux changes.
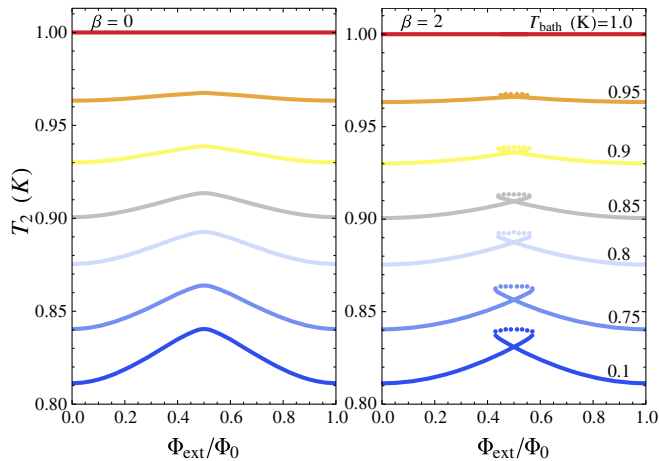
Conversely, for memory applications, robustness against small external-field fluctuations is desirable. In fact, a system showing a clear hysteresis can promptly find applications as memory elements. In superconducting devices, it is natural to use persistent currents or magnetic flux in a superconducting loop for binary information storage [30]. Specifically, in a SQUID, the logical 0 and 1 usually correspond to zero and a single flux quantum in the loop, respectively. More recently, other superconducting tunnel-junction-based memory elements were suggested [31–35]. A memory based on a thermally biased inductive SQUID could take advantage of the clear hysteretic behavior of the temperature of the cold electrode for proper values of the external flux. For instance, the thermal jump $\Delta T_2 \sim 20$ mK, for $T_1 = 0.84$ K, $T_{bath} = 0.1$ K, and $\Phi_{ext} \simeq 0.63\Phi_0$, shown in Fig. 8(c) allows us to clearly distinguish a "heat-bit 1," associated with the state where $k = 0$, from a "heat-bit 0" for the state with $k = 1$.

It is worth noting that the dynamics of a SQUID in the so-called adiabatic regime strongly depends on whether the frequency ω_{ext} of the external magnetic flux is smaller than both the cutoff frequency of the SQUID loop, $\omega_{cut} = R/L$, and the junction characteristic frequency [18], $\omega_c = 2\pi R_a I_J^a/\Phi_0$. The time of a quantum transition, $k \to k \pm 1$, as the flux through the SQUID suddenly changes is given by ω_{cut}^{-1} or by ω_c^{-1}, depending on which is larger [26]. Therefore, in the adiabatic regime, the sweep frequency ω_{ext} must be much slower than the characteristic time for a flux transition.

Finally, the speed of modulation of the temperature T_2 depends mainly on the relaxation time $\tau_{e\text{-ph}}$ required by the quasiparticle in S_2 to thermalize with lattice phonons since the $R_a C$ time constant of the junctions forming the SQUID can be reduced more than $\tau_{e\text{-ph}}$ by properly choosing the system parameters. In particular, in the 0.5 K ÷ 1 K temperature range, $\tau_{e\text{-ph}}^{-1}$ is on the order of approximately 1–10 MHz for Al [10,36], whereas, at lower T_{bath}'s, it is drastically reduced owing to an increased electron-phonon relaxation time [36,37]. However, we stress that $\tau_{e\text{-ph}}^{-1}$ can be enhanced by using other superconductors with higher electron-phonon coupling than Al, like, for instance, tantalum [10,37]. Moreover, the use of superconductors with higher T_c's permits higher working temperatures, resulting in a further enhancement of the electron-phonon relaxation frequency. Finally, the fine-tuning of the system could allow memory applications also at gigahertz frequencies (see the Appendix).

IV. CONCLUSIONS

In this paper, we study the modulation of the temperature in a thermally biased SQUID with a non-negligible inductance of the superconducting ring when the external magnetic flux through the device, Φ_{ext}, is changed. Specifically, we analyze the thermal current flowing in

FIG. 9. Quasiparticle temperature T_2 vs Φ_{ext} calculated for a few values of T_{bath} at $T_1 = 1$ K for $\alpha = 0.75$, where $\beta = 0.0$ and $\beta = 2$ [(a) and (b), respectively]. Dotted curves represent the unstable states in the hysteretic mode.

the SQUID by varying the values of the hysteresis parameter β, which is proportional to the product of the inductance and the critical current of a JJ, and the ratio α between the JJ's critical currents. Moreover, we investigate the steady temperature, T_2, of the cold electrode for several temperatures of the heater and the thermal bath. For proper values of β, the SQUID behaves hysteretically as the external flux is properly swept. We observe temperature modulation as a function of Φ_{ext} and hysteretic transitions in the thermal current flowing through the junctions. This hysteretic behavior directly reflects on the temperature T_2, as the thermal contact with both the other electrode and the phonon bath is taken into account in the thermal model.

Accordingly, as Φ_{ext} induces a transition in the number of flux quanta through the SQUID ring, pronounced jumps in T_2 occur, up to $\Delta T_2 \sim 20$ mK, for $T_1 = 0.84$ K and $T_{bath} = 0.1$ K in a realistic Al-based proposed setup. The emergence of this thermal hysteresis suggests the use of a thermally biased inductive SQUID as a memory element, in which the input- and output-related variables are the external magnetic flux and the temperature of a branch of the SQUID. Such memory could work even in a range of frequencies on the order of gigahertz by properly choosing the superconductors forming the SQUID. The proposed systems could be easily implemented by standard nano-fabrication techniques through the setup proposed for the SQUID-based Josephson heat interferometer [2].

ACKNOWLEDGMENTS

APPENDIX: HEAT RELAXATION TIME SCALE

The thermal relaxation time scale of the system can be estimated by the time for the superconductor, at the temperature T_{hot}, to reach the temperature $(T_{bath} + T_{hot})/2$ as the thermal contact with a phonon bath is taken into account. The thermal balance equation for a superconductor in thermal contact with a phonon bath can be written as

$$-\dot{Q}_{e\text{-ph}}(T, T_{bath}) = C_v(T)\frac{dT}{dt}, \qquad (A1)$$

where $\dot{Q}_{e\text{-ph}}$ is given by Eq. (21) and the rhs of the equation represents the variations of the internal energy of the system.
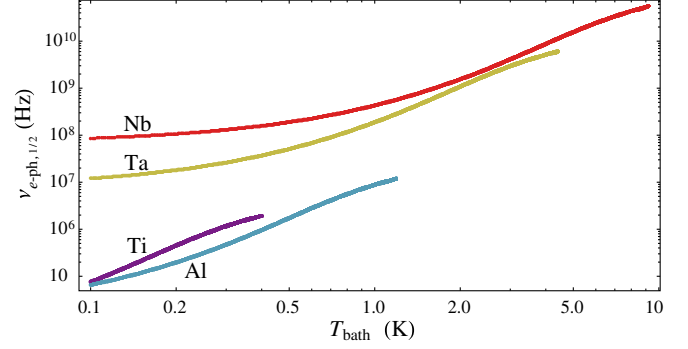

FIG. 10. Electron-phonon relaxation frequency, $\nu_{e\text{-ph},1/2} = \tau_{e\text{-ph},1/2}^{-1}$, as a function of the bath temperature, T_{bath}, for $N_F = 10^{47}$ J^{-1} m^{-3} and by choosing $T_{hot} = (T_{bath} + T_c)/2$, for several superconductors, i.e., Ti, Al, Ta, and Nb.

In Eq. (A1), $C_v(T)$ is the heat capacity given by [38]

$$C_v(T) = \mathcal{V}T\frac{dS(T)}{dT}, \qquad (A2)$$

where $\mathcal{V}$ is the volume and $S(T)$ is the electronic entropy of the superconductor [38–40]

$$S = -4k_B N_F \int_0^\infty d\varepsilon \mathcal{N}(\varepsilon, T)\{[1 - f(\varepsilon, T)]\log[1 - f(\varepsilon, T)] + f(\varepsilon, T)\log f(\varepsilon, T)\}, \qquad (A3)$$

with N_F being the density of states at the Fermi energy. From Eq. (A1), the electron-phonon relaxation time from the temperature T_{hot} to the temperature $(T_{bath} + T_{hot})/2$ can be evaluated as

$$\tau_{e\text{-ph},1/2} = \int_{\frac{T_{bath}+T_{hot}}{2}}^{T_{hot}} \frac{C_v(T)}{\dot{Q}_{e\text{-ph}}(T, T_{bath})}dT. \qquad (A4)$$

From Eqs. (21) and (A4), we observe that the electron-phonon relaxation frequency, $\nu_{e\text{-ph},1/2} = \tau_{e\text{-ph},1/2}^{-1}$, depends on both the working temperatures and the characteristics of the superconductor, such as the electron-phonon coupling constant Σ and the critical temperature T_c.

The behavior of $\nu_{e\text{-ph},1/2}$ as a function of the bath temperature, for $N_F = 10^{47}$ J^{-1} m^{-3} and by choosing $T_{hot} = (T_{bath} + T_c)/2$, is shown in Fig. 10 for several superconductors. Specifically, the results in Fig. 10 are obtained for Ti ($T_c = 0.4$ K, $\Sigma = 1.33\,10^9$ Wm^{-3} K^{-5} [16]), Al ($T_c = 1.19$ K, $\Sigma = 0.3\,10^9$ Wm^{-3} K^{-5} [16]), Ta ($T_c = 4.43$ K, $\Sigma = 3\,10^9$ Wm^{-3} K^{-5} [10,37]), and Nb ($T_c = 9.2$ K, by supposing $\Sigma = 3\,10^9$ Wm^{-3} K^{-5}). We observe that $\nu_{e\text{-ph},1/2} \lesssim 10$ MHz for Al, whereas e-ph relaxation frequencies on the order of gigahertz can be achieved at $T_{bath} \sim 2$ K for both Ta and Nb.

[1] K. Maki and A. Griffin, Entropy Transport Between Two Superconductors by Electron Tunneling, Phys. Rev. Lett. **15**, 921 (1965).

[2] F. Giazotto and M. J. Martínez-Pérez, The Josephson heat interferometer, Nature (London) **492**, 401 (2012).

[3] M. J. Martínez-Pérez and F. Giazotto, Fully balanced heat interferometer, Appl. Phys. Lett. **102**, 092602 (2013).

[4] M. J. Martínez-Pérez and F. Giazotto, Efficient phase-tunable Josephson thermal rectifier, Appl. Phys. Lett. **102**, 182602 (2013).

[5] M. J. Martínez-Pérez and F. Giazotto, A quantum diffractor for thermal flux, Nat. Commun. **5**, 3579 (2014).

[6] M. J. Martínez-Pérez, P. Solinas, and F. Giazotto, Coherent caloritronics in Josephson-based nanocircuits, J. Low Temp. Phys. **175**, 813 (2014).

[7] A. Fornieri, C. Blanc, R. Bosisio, S. D'Ambrosio, and F. Giazotto, Nanoscale phase engineering of thermal transport with a Josephson heat modulator, Nat. Nanotechnol. **11**, 258 (2016).

[8] A. Fornieri, G. Timossi, P. Virtanen, P. Solinas, and F. Giazotto, 0-π phase-controllable thermal Josephson junction, Nat. Nanotechnol., DOI: 10.1038/nnano.2017.25 (2017).

[9] A. Fornieri and F. Giazotto, Towards phase-coherent caloritronics in superconducting quantum circuits, arXiv: 1610.01013.

[10] F. Giazotto and M. J. Martínez-Pérez, Phase-controlled superconducting heat-flux quantum modulator, Appl. Phys. Lett. **101**, 102601 (2012).

[11] G. D. Guttman, B. Nathanson, E. Ben-Jacob, and D. J. Bergman, Phase-dependent thermal transport in Josephson junctions, Phys. Rev. B **55**, 3849 (1997).

[12] G. D. Guttman, E. Ben-Jacob, and D. J. Bergman, Interference effect heat conductance in a Josephson junction and its detection in an rf SQUID, Phys. Rev. B **57**, 2717 (1998).

[13] E. Zhao, T. Löfwander, and J. A. Sauls, Phase Modulated Thermal Conductance of Josephson Weak Links, Phys. Rev. Lett. **91**, 077003 (2003).

[14] E. Zhao, T. Löfwander, and J. A. Sauls, Heat transport through Josephson point contacts, Phys. Rev. B **69**, 134503 (2004).

[15] D. Golubev, T. Faivre, and J. P. Pekola, Heat transport through a Josephson junction, Phys. Rev. B **87**, 094522 (2013).

[16] F. Giazotto, T. T. Heikkilä, A. Luukanen, A. M. Savin, and J. P. Pekola, Opportunities for mesoscopics in thermometry and refrigeration: Physics and applications, Rev. Mod. Phys. **78**, 217 (2006).

[17] B. Frank and W. Krech, Electronic cooling in superconducting tunnel junctions, Phys. Lett. A **235**, 281 (1997).

[18] A. Barone and G. Paternò, *Physics and Applications of the Josephson Effect* (Wiley, New York, 1982).

[19] R. C. Dynes, V. Narayanamurti, and J. P. Garno, Direct Measurement of Quasiparticle-Lifetime Broadening in a Strong-Coupled Superconductor, Phys. Rev. Lett. **41**, 1509 (1978).

[20] M. J. Martínez-Pérez, A. Fornieri, and F. Giazotto, Rectification of electronic heat current by a hybrid thermal diode, Nat. Nanotechnol. **10**, 303 (2015).

[21] A. Fornieri, G. Timossi, R. Bosisio, P. Solinas, and F. Giazotto, Negative differential thermal conductance and heat amplification in superconducting hybrid devices, Phys. Rev. B **93**, 134508 (2016).

[22] F. Giazotto and J. P. Pekola, Josephson tunnel junction controlled by quasiparticle injection, J. Appl. Phys. **97**, 023908 (2005).

[23] S. Tirelli, A. M. Savin, C. P. Garcia, J. P. Pekola, F. Beltram, and F. Giazotto, Manipulation and Generation of Supercurrent in Out-of-Equilibrium Josephson Tunnel Nanojunctions, Phys. Rev. Lett. **101**, 077004 (2008).

[24] R. Bosisio, P. Solinas, A. Braggio, and F. Giazotto, Photonic heat conduction in Josephson-coupled Bardeen-Cooper-Schrieffer superconductors, Phys. Rev. B **93**, 144512 (2016).

[25] J. B. Majer, J. R. Butcher, and J. E. Mooij, Simple phase bias for superconducting circuits, Appl. Phys. Lett. **80**, 3638 (2002).

[26] J. Clarke and A. Braginski, *The SQUID Handbook: Fundamentals and Technology of SQUIDs and SQUID Systems* (Wiley, New York, 2004), Vol. 1.

[27] M. Bo, T. Zhong-Kui, M. Shu-Chao, D. Yuan-Dong, and W. Fu-Ren, Basic properties of an rf SQUID involving two Josephson junctions connected in series, Chin. Phys. **13**, 1226 (2004).

[28] A. V. Timofeev, C. P. García, N. B. Kopnin, A. M. Savin, M. Meschke, F. Giazotto, and J. P. Pekola, Recombination-Limited Energy Relaxation in a Bardeen-Cooper-Schrieffer Superconductor, Phys. Rev. Lett. **102**, 017003 (2009).

[29] J. Clarke and R. H. Koch, The impact of high-temperature superconductivity on SQUID magnetometers, Science **242**, 217 (1988).

[30] J. Matisoo, Overview of Josephson technology logic and memory, IBM J. Res. Dev. **24**, 113 (1980).

[31] S. Peotta and M. Di Ventra, Superconducting Memristors, Phys. Rev. Applied **2**, 034011 (2014).

[32] S. N. Shevchenko, Y. V. Pershin, and F. Nori, Qubit-Based Memcapacitors and Meminductors, Phys. Rev. Applied **6**, 014006 (2016).

[33] J. Salmilehto, F. Deppe, M. Di Ventra, M. Sanz, and E. Solano, Quantum memristors with superconducting circuits, Sci. Rep. **7**, 42044 (2017).

[34] C. Guarcello, P. Solinas, M. Di Ventra, and F. Giazotto, Solitonic Josephson-based meminductive systems, Sci. Rep. **7**, 46736 (2017).

[35] P. Pfeiffer, I. Egusquiza, M. Di Ventra, M. Sanz, and E. Solano, Quantum memristors, Sci. Rep. **6**, 29507 (2016).

[36] S. B. Kaplan, C. C. Chi, D. N. Langenberg, J. J. Chang, S. Jafarey, and D. J. Scalapino, Quasiparticle and phonon lifetimes in superconductors, Phys. Rev. B **14**, 4854 (1976).

[37] R. Barends, J. J. A. Baselmans, S. J. C. Yates, J. R. Gao, J. N. Hovenier, and T. M. Klapwijk, Quasiparticle Relaxation in Optically Excited High-Q Superconducting Resonators, Phys. Rev. Lett. **100**, 257002 (2008).

[38] H. Kusunose, Quasiclassical theory of superconducting states under magnetic fields: Thermodynamic properties, Phys. Rev. B **70**, 054509 (2004).

[39] H. Rabani, F. Taddei, O. Bourgeois, R. Fazio, and F. Giazotto, Phase-dependent electronic specific heat of mesoscopic Josephson junctions, Phys. Rev. B **78**, 012503 (2008).

[40] P. Solinas, R. Bosisio, and F. Giazotto, Microwave quantum refrigeration based on the Josephson effect, Phys. Rev. B **93**, 224521 (2016).